Journal of Computational Physics 473 (2023) 111723

Contents lists available at ScienceDirect

Journal of Computational Physics

www.elsevier.com/locate/jcp

A fast, high-order numerical method for the simulation of single-excitation states in quantum optics

Jeremy G. Hoskins [a], Jason Kaye [b,c,*], Manas Rachh [b], John C. Schotland [d]

[a] Department of Statistics, University of Chicago, Chicago, IL 60637, USA
[b] Center for Computational Mathematics, Flatiron Institute, New York, NY 10010, USA
[c] Center for Computational Quantum Physics, Flatiron Institute, New York, NY 10010, USA
[d] Department of Mathematics and Department of Physics, Yale University, New Haven, CT 06511, USA

ARTICLE INFO

Article history:
Received 3 March 2022
Received in revised form 6 October 2022
Accepted 22 October 2022
Available online 26 October 2022

Keywords:
Quantum optics
Nonlocal partial differential equations
Volterra integro-differential equations
Sum of exponentials compression

ABSTRACT

We consider the numerical solution of a nonlocal partial differential equation which describes the phenomenon of collective spontaneous emission in a two-level atomic system containing a single photon. We reformulate the problem as an integro-differential equation for the atomic degrees of freedom, and describe an efficient solver for the case of a Gaussian atomic density. The problem of history dependence arising from the integral formulation is addressed using sum-of-exponentials history compression. We demonstrate the solver on two systems of physical interest: in the first, an initially-excited atom decays into a photon by spontaneous emission, and in the second, a photon pulse is used to an excite an atom, which then decays.

1. Introduction

Many-body problems in quantum optics are of interest in the study of cold-atom systems, quantum waveguides, and quantum semiconductor devices, among others, with applications to quantum computing, quantum information processing, and precision measurements [1–8]. The simplest such problem arises in a system of two-level atoms interacting with a single photon. In this setting, the propagation of a single-photon state is governed by the system of partial differential equations [9]

$$\begin{aligned} i\partial_t u(x,t) &= c(-\Delta)^{1/2}u(x,t) + g\rho(x)a(x,t), \quad (x,t) \in \mathbb{R}^{d+1}, \\ i\partial_t a(x,t) &= \Omega a(x,t) + g u(x,t). \end{aligned} \tag{1}$$

Here u is the probability amplitude for creating a photon, a is the probability amplitude for exciting an atom, ρ is the atomic number density, Ω is the atomic resonance frequency, and g is the atom-field coupling constant. The amplitudes obey the normalization condition

$$\int_{\mathbb{R}^d} \left(|u(x,t)|^2 + \rho(x)|a(x,t)|^2 \right) dx = 1, \tag{2}$$

* Corresponding author.
E-mail address: jkaye@flatironinstitute.org (J. Kaye).

https://doi.org/10.1016/j.jcp.2022.111723
0021-9991/

which has the interpretation that $|u|^2$ is the one-photon probability density and that $\rho|a|^2$ is the atomic probability density. In physical terms, (1) describes the process of collective spontaneous emission. That is, suppose that an atom is initially in its excited state and there are no photons present in the field. The atom can then decay, transferring its excitation to the field, which can then excite the remaining atoms, causing them to decay in a similar manner and so on.

Eq. (1) has been investigated in several cases of interest, including a single atom, a uniform medium of constant density, and a statistically homogeneous random medium [9]. This paper is the first in a series devoted to the analysis and numerical solution of (1). We note that standard numerical methods are not readily applicable to this problem, which was originally introduced in Ref. [9], and to our knowledge this is the first paper which discusses its numerical solution. In order to illustrate the difficulty, we outline the drawbacks of two possible approaches.

Physical domain discretization We could consider discretizing the first equation in (1) directly in physical space using a finite difference or finite element method, and then solve the resulting system of ODEs. However, the nonlocal character of the fractional Laplacian operator $(-\Delta)^{1/2}$, which is given by

$$(-\Delta)^{1/2} f(x) = \frac{\Gamma\left(\frac{d+1}{2}\right)}{\pi^{\frac{d+1}{2}}} \int_{\mathbb{R}^d} \frac{f(x) - f(y)}{|x-y|^{d+1}}\, dy,$$

leads to two related difficulties. First, any discretization of the operator would produce a dense matrix, leading to a large cost per time step in the absence of suitable fast algorithms. Perhaps more importantly, the photon field $u(x,t)$ would need to be discretized on a domain containing its full numerical support, which spreads rapidly. This would, in practice, limit simulations to very short times. One possible remedy would be to truncate the computational domain and impose suitable artificial outgoing boundary conditions, but for large systems the cost of discretizing the photon field in the truncated computational domain would remain an issue.

Fourier domain discretization The above observations suggest working in the Fourier domain, in which the action of the fractional Laplacian is diagonal:

$$(-\Delta)^{1/2} f(x) = \frac{1}{(2\pi)^d} \int_{\mathbb{R}^d} e^{i\xi\cdot x} |\xi|\, \widehat{f}(\xi)\, d\xi,$$

where $\widehat{f}(\xi)$ is the Fourier transform of f, which is defined by

$$\widehat{f}(\xi) = \int_{\mathbb{R}^d} e^{-i\xi\cdot x} f(x)\, dx.$$

One could design a Fourier pseudospectral method, such that at each time step, the action of the fractional Laplacian is computed in the Fourier domain, and the product $\rho(x)a(x,t)$ is computed in the physical domain. Such methods are commonly used to solve PDEs of evolution, such as the time-dependent Schrödinger equation, involving a Laplacian term diagonal in the Fourier domain, and a second term which is more easily computed in the physical domain [10,11]. Here, we encounter the Fourier domain manifestation of the same problem. Namely, spreading in the physical domain corresponds to oscillation in the Fourier domain, and we obtain a photon amplitude which becomes more and more oscillatory in the Fourier domain as time progresses. As a result, one would expect the computational cost to scale at least quadratically with the propagation time.

Our approach is to recast (5) as a Volterra integral equation for the atomic amplitude. In particular, we eliminate the photon field using a suitable Green's function, obviating the need to discretize large spatial domains. The number of degrees of freedom in the required discretization depends only on the size of the support of ρ. As such, our method enables fast and accurate simulations over long times.

We begin by constructing the Green's function for the homogeneous part of the equation describing u, which satisfies

$$\begin{aligned} i\partial_t G(x,t) &= c(-\Delta)^{1/2} G(x,t) \\ \lim_{t\to 0^+} G(x,t) &= \delta(x). \end{aligned} \tag{3}$$

The solution in the Fourier domain is given by

$$\widehat{G}(\xi,t) = e^{-ic|\xi|t}. \tag{4}$$

This implies that in the case $g = 0$, $u(\xi,t)$ is given by

$$u(\xi,t) = \widehat{G}(\xi,t)\widehat{u_0}(\xi) = e^{-ic|\xi|t}\widehat{u_0}(\xi),$$

from which the oscillatory behavior is clear.

We wish to make use of the Green's function representation of $u(x,t)$, but to avoid discretizing it in the Fourier domain. To proceed, we rewrite (1) as

$$\begin{aligned} i\partial_t u(x,t) &= c(-\Delta)^{1/2}u(x,t) + \frac{g}{\sigma^d}\rho(x/\sigma)a(x,t), \\ i\partial_t a(x,t) &= \Omega a(x,t) + g u(x,t), \\ u(x,0) &= u_0(x), \\ a(x,0) &= a_0(x), \end{aligned} \tag{5}$$

where the density ρ has been rescaled by the length σ, which characterizes the spatial extent of the atoms. Next we reformulate (5) as a Volterra integro-differential equation in the unknown $b(x,t) = \frac{\rho(x/\sigma)}{\sigma^d}a(x,t)$ alone. Applying the Duhamel principle to the first equation in (5) gives

$$u(x,t) = \int_{\mathbb{R}^d} G(x-y,t)u_0(y)\,dy - i\frac{g}{\sigma^d}\int_0^t\int_{\mathbb{R}^d} G(x-y,t-s)\rho(y/\sigma)a(y,s)\,dy\,ds. \tag{6}$$

Substituting the above into the second equation in (5) and multiplying by $\rho(x/\sigma)/\sigma^d$ gives

$$\partial_t b(x,t) = -i\Omega b(x,t) - g^2\frac{\rho(x/\sigma)}{\sigma^d}\int_0^t\int_{\mathbb{R}^d} G(x-y,t-s)b(y,s)\,dy\,ds - ig\frac{\rho(x/\sigma)}{\sigma^d}U(x,t), \tag{7}$$

where we have defined

$$U(x,t) = \int_{\mathbb{R}^d} G(x-y,t)u_0(y)\,dy,$$

which is the free evolution of the photon amplitude $u_0(x)$. If (7) is solved, the photon amplitude can be recovered as a matter of post-processing using (6).

The main advantage of solving (7) over the formulations mentioned above is that for a localized density $\rho(x)$, $b(x,t)$ remains localized as well. The price we pay is a dense dependence of the solution $b(x,t)$ on its history $b(x,s)$ for $0 \le s < t$. Indeed, it appears that each time step, we must evaluate the history integral on the right hand side of (7). This leads to an algorithm which, for a given accuracy, has a computational cost scaling as $\mathcal{O}\left(N^2\right)$ in the number N of time steps, and a memory requirement scaling as $\mathcal{O}(N)$. This is a typical challenge associated with the application of Volterra integral operators, and several techniques have been proposed to address it, particularly in the context of solving Volterra integral equations [12–18] and applying Volterra integral operators corresponding to nonlocal transparent boundary conditions [19–24]. We will make use of one such approach – the sum of exponentials approximation method – to obtain a high-order accurate numerical method with $\mathcal{O}(N\log N)$ computational complexity and $\mathcal{O}(\log N)$ memory complexity.

We focus in this article on the case of a Gaussian atomic density in one spatial dimension. There is no fundamental difficulty in extending our method to densities comprised of sums of Gaussians, and to three spatial dimensions. These extensions will be addressed in a forthcoming publication. A generalization to other densities may also be possible, but Gaussian and sum-of-Gaussian densities are a suitable physical model for many systems of contemporary interest. We will see that the present case already exhibits nontrivial dynamics which are expected to appear in three dimensions as well.

This article is organized as follows. In Section 2, we describe the mathematical setup for our numerical method. We describe our high-order time-stepping algorithm in Section 3, and fill in technical details involving the representation and evaluation of certain special functions in Section 4. In Section 5 we present numerical results which demonstrate the accuracy of the method and give insight into the behavior of the solution for two physically meaningful examples. Section 6 concludes with a discussion of several open questions and future research directions.

2. Problem setup

To set up our numerical method we will represent the atom amplitude $a(x,t)$ in the one-dimensional case by an expansion

$$a(x,t) = \sum_{n=0}^{p-1} a_n(t)\,f_n(x/\sigma). \tag{8}$$

Here $\{f_n(x)\}_{n=0}^{p-1}$ are the first p polynomials orthonormal with respect to $\rho(x)$, so that $\{f_n(x/\sigma)\}_{n=0}^{p-1}$ are orthonormal with respect to the scaled density $\rho(x/\sigma)/\sigma$. We will first derive a coupled set of Volterra integral equations (VIEs) for the modal coefficients $a_n(t)$. We will then obtain explicit expressions for the case in which the atomic density ρ is a Gaussian. Finally, we will show how to recover the photon amplitude from the coefficients a_n of the atom amplitude.

2.1. Volterra integral equation for the atomic degrees of freedom

Substituting (8) into (7), integrating against $f_m(x/\sigma)$, and defining

$$U_m(t) = \frac{1}{\sigma}\int_{-\infty}^{\infty} \rho(x/\sigma) f_m(x/\sigma) U(x,t)\,dx,$$

we obtain

$$\dot{a}_m(t) = -i\Omega a_m(t) - \frac{g^2}{\sigma^2}\sum_{n=0}^{p-1}\int_{-\infty}^{\infty} \rho(x/\sigma) f_m(x/\sigma)\int_0^t a_n(s)\int_{-\infty}^{\infty} G(x-y,t-s)\rho(y/\sigma) f_n(y/\sigma)\,dy\,ds\,dx - igU_m(t),$$

where the dot denotes a derivative with respect to time. From (4), we have

$$G(x,t) = \frac{1}{2\pi}\int_{-\infty}^{\infty} e^{i(\xi x - c|\xi|t)}\,d\xi,$$

which gives

$$\begin{aligned}
&\int_{-\infty}^{\infty} \rho(x/\sigma) f_m(x/\sigma)\int_0^t a_n(s)\int_{-\infty}^{\infty} G(x-y,t-s)\rho(y/\sigma) a_n(s) f_n(y/\sigma)\,dy\,ds\,dx \\
&= \frac{1}{2\pi}\int_0^t a_n(s)\int_{-\infty}^{\infty} e^{-ic|\xi|(t-s)}\left(\int_{-\infty}^{\infty} e^{i\xi x}\rho(x/\sigma) f_m(x/\sigma)\,dx\right)\left(\int_{-\infty}^{\infty} e^{-i\xi y}\rho(y/\sigma) f_n(y/\sigma)\,dy\right)d\xi\,ds \\
&= \frac{\sigma^2}{2\pi}\int_0^t a_n(s)\int_{-\infty}^{\infty} e^{-ic|\xi|(t-s)}\widehat{(\rho f_m)}(-\sigma\xi)\widehat{(\rho f_n)}(\sigma\xi)\,d\xi\,ds \\
&= \frac{\sigma^2}{2\pi}\int_0^t a_n(s)\int_0^{\infty} e^{-ic\xi(t-s)}\Phi_{mn}(\sigma\xi)\,d\xi\,ds,
\end{aligned}$$

where

$$\Phi_{mn}(\xi) = \phi_m(\xi)\phi_n(-\xi) + \phi_m(-\xi)\phi_n(\xi)$$

with

$$\phi_n(\xi) = \widehat{(\rho f_n)}(\xi).$$

Defining

$$J_{mn}(t) = \int_0^{\infty} e^{-i\xi t}\Phi_{mn}(\xi)\,d\xi,$$

we obtain

$$\dot{a}_m(t) = -i\Omega a_m(t) - \frac{g^2}{2\pi\sigma}\sum_{n=0}^{p-1}\int_0^t J_{mn}\left(\frac{c}{\sigma}(t-s)\right)a_n(s)\,ds - igU_m(t).$$

The change of variables

$$\alpha_m(t) = e^{i\Omega t}a_m(t) \tag{9}$$

gives

$$\dot{\alpha}_m(t) = -\frac{g^2}{2\pi\sigma}\sum_{n=0}^{p-1}\int_0^t e^{i\Omega(t-s)} J_{mn}\left(\frac{c}{\sigma}(t-s)\right)\alpha_n(s)\,ds - ige^{i\Omega t}U_m(t).$$

Integrating both sides in time and swapping the order of integration yields

$$\alpha_m(t) + \frac{g^2}{2\pi c}\sum_{n=0}^{p-1}\int_0^t K_{mn}\left(\frac{c}{\sigma}(t-s)\right)\alpha_n(s)\,ds = a_m(0) - ig\int_0^t e^{i\Omega s}U_m(s)\,ds \tag{10}$$

with

$$K_{mn}(t) = \int_0^t e^{i\frac{\Omega\sigma}{c}s} J_{mn}(s)\,ds. \tag{11}$$

The above is a collection of coupled second-kind VIEs for $\alpha_m(t)$, $m = 0, \ldots, p-1$, from which $a(x,t)$ can be recovered using (8) and (9).

We pause to consider the calculation of the total probability, given as in (2) by

$$1 = \frac{1}{\sigma}\int_{-\infty}^{\infty} |a(x,t)|^2\,\rho(x/\sigma)\,dx + \int_{-\infty}^{\infty} |u(x,t)|^2\,dx \equiv P_a(t) + P_u(t). \tag{12}$$

Here, we have defined P_a and P_u as the atomic and photonic contributions to the total probability, respectively. It is straightforward to calculate P_a, a quantity of physical interest, within our framework:

$$\begin{aligned} P_a(t) &= \frac{1}{\sigma}\int_{-\infty}^{\infty} |a(x,t)|^2\,\rho(x/\sigma)\,dx \\ &= \frac{1}{\sigma}\sum_{n=0}^{p-1}\sum_{m=0}^{p-1} a_m^*(t)a_n(t)\int_{-\infty}^{\infty} f_m^*(x/\sigma)\,f_n^*(x/\sigma)\rho(x/\sigma)\,dx \\ &= \sum_{n=0}^{p-1}|a_n(t)|^2 = \sum_{n=0}^{p-1}|\alpha_n(t)|^2\,. \end{aligned} \tag{13}$$

2.2. Gaussian atomic density

Let us take the atomic density to be a Gaussian,

$$\rho(x) = \frac{e^{-x^2}}{\sqrt{\pi}}.$$

Then

$$f_n(x) = \frac{H_n(x)}{\sqrt{2^n n!}},$$

with H_n the Hermite polynomial of degree n, defined by

$$H_n(x)e^{-x^2} = (-1)^n\frac{d^n}{dx^n}e^{-x^2}. \tag{14}$$

The above follows from the formula [25, Eqn. 7.374.1]

$$\int_{-\infty}^{\infty} H_m(x)H_n(x)e^{-x^2}\,dx = \sqrt{\pi}2^n n!\delta_{mn}.$$

Taking the Fourier transform of (14) gives

$$\phi_n(\xi) = \widehat{(\rho f_n)}(\xi) = \frac{(-i)^n}{\sqrt{2^n n!}}\xi^n e^{-\xi^2/4}. \tag{15}$$

In particular, we find that $\Phi_{mn}(\xi) = 0$ if m is even and n is odd or vice versa, and otherwise

$$\Phi_{mn}(\xi) = 2(-1)^m \phi_m(\xi)\phi_n(\xi) = \frac{(-1)^m(-i)^{m+n}}{\sqrt{2^{m+n-2}m!n!}}\xi^{m+n}e^{-\xi^2/2}.$$

We remark that the vanishing of Φ_{mn} for odd $m+n$ is a consequence of the symmetry of ρ. For more general densities, all Φ_{mn} will be non-zero. The kernel J_{mn} is then given by

$$J_{mn}(t) = \frac{(-1)^m(-i)^{m+n}}{\sqrt{2^{m+n-2}m!n!}}\int_0^\infty \xi^{m+n}e^{-\xi^2/2-i\xi t}\,d\xi$$

if m and n are even or odd together, and zero otherwise. We define

$$j_n(t) = \frac{2}{\Gamma\left(\frac{n+1}{2}\right)}\int_0^\infty \xi^n e^{-\xi^2-i\xi t}\,d\xi. \tag{16}$$

Here Γ is the Gamma function, and the normalization is chosen so that $j_n(0) = 1$. A change of variables gives

$$J_{mn}(t) = \begin{cases} (-1)^m(-i)^{m+n}\frac{\Gamma\left(\frac{m+n+1}{2}\right)}{\sqrt{\frac{m!n!}{2}}}j_{m+n}\left(\sqrt{2}t\right) & \text{if } m+n \equiv 0 \pmod 2 \\ 0 & \text{otherwise.} \end{cases}$$

We also define

$$k_n(t) = \int_0^t e^{i\frac{\Omega\sigma}{c}s}j_n(\sqrt{2}s)\,ds \tag{17}$$

so that

$$K_{mn}(t) = \begin{cases} (-1)^m(-i)^{m+n}\frac{\Gamma\left(\frac{m+n+1}{2}\right)}{\sqrt{\frac{m!n!}{2}}}k_{m+n}(t) & \text{if } m+n \equiv 0 \pmod 2 \\ 0 & \text{otherwise.} \end{cases} \tag{18}$$

2.3. Recovering the photon amplitude

The photon amplitude is given by (6). The first term, $U(x,t)$, describes the contribution to the amplitude of the initial photon field configuration, and is straightforward to compute by Fourier transform as long as u_0 is well-behaved.

For the second term, we write

$$\begin{aligned} u(x,t) - U(x,t) &= -\frac{ig}{\sigma}\int_0^t\int_{-\infty}^\infty G(x-y,t-s)\rho(y/\sigma)a(y,s)\,dy\,ds \\ &= -\frac{ig}{2\pi\sigma}\int_0^t\int_{-\infty}^\infty e^{-ic|\xi|(t-s)}e^{i\xi x}\int_{-\infty}^\infty e^{-i\xi y}\rho(y/\sigma)a(y,s)\,dy\,d\xi\,ds \\ &= -\frac{ig}{2\pi\sigma}\sum_{n=0}^{p-1}\int_0^t a_n(s)\int_{-\infty}^\infty e^{-ic|\xi|(t-s)}e^{i\xi x}\int_{-\infty}^\infty e^{-i\xi y}\rho(y/\sigma)f_n(y/\sigma)\,dy\,d\xi\,ds \\ &= -\frac{ig}{2\pi\sigma}\sum_{n=0}^{p-1}\int_0^t a_n(s)\int_{-\infty}^\infty e^{-ic|\xi|(t-s)/\sigma}e^{i\xi x/\sigma}\phi_n(\xi)\,d\xi\,ds \\ &= -\frac{ig}{2\pi\sigma}\sum_{n=0}^{p-1}\int_0^t a_n(s)\int_0^\infty e^{-ic\xi(t-s)/\sigma}\left(e^{i\xi x/\sigma}\phi_n(\xi) + e^{-i\xi x/\sigma}\phi_n(-\xi)\right)d\xi\,ds. \end{aligned}$$

Once we have solved (10), we can recover the coefficients $a_m(t)$ from (9), and compute the photon amplitude as above. In the case of a Gaussian atomic density, (15) and (16) yield

$$
\begin{aligned}
&u(x,t) - U(x,t) \\
&\quad = -\frac{ig}{2\pi\sigma} \sum_{n=0}^{p-1} \frac{(-i)^n}{\sqrt{2^n n!}} \int_0^t a_n(s) \int_0^\infty e^{-ic\xi(t-s)/\sigma - \xi^2/4} \left(e^{i\xi x/\sigma} \xi^n + (-1)^n e^{-i\xi x/\sigma} \xi^n \right) d\xi \, ds \\
&\quad = -\frac{ig}{2\pi\sigma} \sum_{n=0}^{p-1} \frac{(-i)^n 2^{\frac{n}{2}} \Gamma\left(\frac{n+1}{2}\right)}{\sqrt{n!}} \int_0^t a_n(s) \left[j_n\left(\frac{2\,(c(t-s)-x)}{\sigma} \right) \right. \\
&\qquad \left. + (-1)^n j_n\left(\frac{2\,(c(t-s)+x)}{\sigma} \right) \right] ds,
\end{aligned}
$$

after some manipulation.

3. Discretization and numerical solution

We use a high-order implicit Gauss-Legendre collocation method to discretize and solve the VIE (10). As is typical with VIEs, the primary computational bottleneck is the evaluation of history integrals at each time step. The naive cost of these evaluations scales quadratically with the total number of time steps, but we will show that it can reduced by splitting the history integrals into local and history parts, and deriving recurrences for the latter using sum-of-exponentials representations of the kernels $K_{mn}(t)$.

We begin by describing our discretization scheme. We divide the time interval $[0, T]$ into N uniform subintervals $\{[(j-1)\Delta t, j\Delta t]\}_{j=0}^{N-1}$, with $\Delta t = T/N$. Let $\{\tau_k\}_{k=0}^{q-1}$ be the collection of q Gauss-Legendre nodes, rescaled and shifted to the interval $[0, \Delta t]$. We place q Gauss-Legendre nodes on each subinterval, so that the full set of collocation nodes is given by $t_{jk} = (j-1)\Delta t + \tau_k$ for $j = 1, \ldots, N$ and $k = 0, \ldots, q-1$.

We denote the numerical approximation of $\alpha_m(t_{jk})$ by $\alpha_{m,j,k}$. In addition to this so-called grid representation of the numerical solution, we will also sometimes represent the numerical solution on a subinterval $[(j-1)\Delta t, j\Delta t]$ by

$$
\alpha(t) \approx \sum_{k=0}^{q-1} \widehat{\alpha}_{m,j,k} P_k^j(t), \tag{19}
$$

where $P_k^j(t)$ is the Legendre polynomial of degree k on the interval $[(j-1)\Delta t, j\Delta t]$; that is, $P_k^j(t) = P_k(t-(j-1)\Delta t)$, where $P_k(\tau)$ is the Legendre polynomial of degree k on $[0, \Delta t]$. One can transform back and forth between the grid representation $\alpha_{m,j,k}$ and the Legendre coefficient representation $\widehat{\alpha}_{m,j,k}$ on the jth subinterval by interpolation of the expansion (19) at the Gauss-Legendre nodes t_{jk}. Indeed, we have

$$
\alpha_{m,j,k} = \sum_{l=0}^{q-1} P_l^j(t_{jk}) \widehat{\alpha}_{m,j,l} = \sum_{l=0}^{q-1} P_l(\tau_k) \widehat{\alpha}_{m,j,l},
$$

and the matrix $\mathcal{T}_{kl} = P_l(\tau_k)$ is well-conditioned [26]. We can therefore obtain the grid representation from the coefficient representation by applying $\mathcal{T}$, and the coefficient representation from the grid representation by applying $\mathcal{T}^{-1}$. We refer to $\mathcal{T}^{-1}$ as the *discrete Legendre transform* matrix.

We split the integral operator in (10) into three pieces:

$$
\begin{aligned}
\int_0^t K_{mn}(t-s)\alpha_n(s)\,ds &= \left(\int_{(j-1)\Delta t}^{t} + \int_{t_j^*}^{(j-1)\Delta t} + \int_0^{t_j^*} \right) K_{mn}\left(\frac{c}{\sigma}(t-s) \right) \alpha_n(s)\,ds \\
&\equiv C_{m,n,j}(t) + L_{m,n,j}(t) + H_{m,n,j}(t).
\end{aligned}
$$

Here, the labels of the three integrals stand for current-time, local, and history, respectively. We define $t_j^* = \max(0, (j-M)\Delta t)$ for a fixed positive integer $M \le N$, which is the number of time steps in the current and local intervals in the time domain. The local interval is empty initially, and grows to a maximum length of $(M-1)\Delta t$, whereas the history interval is empty until $j = M+1$, after which it grows by Δt each time step. The splitting into local and history parts is made because the sum-of-exponentials representation of $K_{mn}(t)$ is only valid sufficiently far into the history, and later M will be chosen based on this domain of validity. The further splitting off of the current time part is made to conveniently address implicit time-stepping.

To discretize, we use the notation $C_{m,n,j,k} \approx C_{m,n,j}(t_{jk}) \equiv C_{m,n,j}((j-1)\Delta t + \tau_k)$, and similarly for $L_{m,n,j,k}$ and $H_{m,n,j,k}$. Then rearranging and evaluating at $t = t_{jk}$, the discretization of the VIE (10) can be written as

$$\alpha_{m,j,k} + \frac{g^2}{2\pi c}\sum_{n=1}^{p} C_{m,n,j,k} = -\frac{g^2}{2\pi c}\sum_{n=1}^{p}\left(L_{m,n,j,k} + H_{m,n,j,k}\right) + f_m(t_{jk}) \tag{20}$$

where we consider $f_m(t) = a_m(0) - ig\int_0^t e^{i\Omega s}U_m(s)\,ds$ as a known source term. We note that at a given time step j_0, all of the quantities on the right-hand side depend on the numerical solution $\alpha_{m,j,k}$ computed only in the first $j_0 - 1$ time steps, $0 \le j \le j_0 - 1$, whereas the left hand side depends on the current-time solution $\alpha_{m,j_0,k}$.

3.1. The current-time term

We have

$$\begin{aligned}
C_{m,n,j,k} &= \int_{(j-1)\Delta t}^{t_{jk}} K_{mn}\left(\frac{c}{\sigma}\left(t_{jk}-s\right)\right)\alpha_n(s)\,ds \\
&= \sum_{l=0}^{q-1}\widehat{\alpha}_{n,j,l}\int_{(j-1)\Delta t}^{t_{jk}} K_{mn}\left(\frac{c}{\sigma}\left(t_{jk}-s\right)\right)P_l^j(s)\,ds \\
&= \sum_{l=0}^{q-1}\widehat{\alpha}_{n,j,l}\int_{0}^{\tau_k} K_{mn}\left(\frac{c}{\sigma}\left(\tau_k-s\right)\right)P_l(s)\,ds \\
&= \sum_{l=0}^{q-1}\widehat{\mathcal{C}}_{m,n,k,l}\widehat{\alpha}_{n,j,l},
\end{aligned}$$

where $\widehat{\mathcal{C}}_{m,n,k,l} = \int_0^{\tau_k} K_{mn}\left(\frac{c}{\sigma}\left(\tau_k - s\right)\right)P_l(s)\,ds$. For each fixed m and n, the array $\widehat{\mathcal{C}}_{m,n,k,l}$ can be precomposed with the discrete Legendre transform matrix $\mathcal{T}^{-1}$, defined above, to obtain an array $\mathcal{C}_{m,n,k,l}$ with

$$C_{m,n,j,k} = \sum_{l=0}^{q-1}\mathcal{C}_{m,n,k,l}\alpha_{n,j,l}. \tag{21}$$

This allows us to work directly with the grid representation of α_n.

The p^2q^2 quantities $\widehat{\mathcal{C}}_{m,n,k,l}$, and therefore $\mathcal{C}_{m,n,k,l}$, can be precomputed and stored. By plugging the expression (18) for $K_{mn}(t)$ in terms of $k_{m+n}(t)$ into the definition of $\widehat{\mathcal{C}}_{m,n,k,l}$, we observe that this can be accomplished by computing only pq^2 integrals – corresponding to the different choices of even $m+n$ for $m, n = 0, \ldots, p-1$ – and scaling the results by constants depending on m and n.

3.2. The local term

We first split the local term into integrals over the subintervals defining each time step, and then take a similar approach as for the current-time term:

$$\begin{aligned}
L_{m,n,j,k} &= \int_{t_j^*}^{(j-1)\Delta t} K_{mn}\left(\frac{c}{\sigma}\left(t_{jk}-s\right)\right)\alpha_n(s)\,ds \\
&= \sum_{\nu=\max(0,M-j)}^{M-2}\int_{(j-M+\nu)\Delta t}^{(j-M+\nu+1)\Delta t} K_{mn}\left(\frac{c}{\sigma}\left(t_{jk}-s\right)\right)\alpha_n(s)\,ds \\
&= \sum_{\nu=\max(0,M-j)}^{M-2}\sum_{l=0}^{q-1}\widehat{\alpha}_{n,j-M+\nu+1,l}\int_{(j-M+\nu)\Delta t}^{(j-M+\nu+1)\Delta t} K_{mn}\left(\frac{c}{\sigma}\left(t_{jk}-s\right)\right)P_l^{j-M+\nu+1}(s)\,ds \\
&= \sum_{\nu=\max(0,M-j)}^{M-2}\sum_{l=0}^{q-1}\widehat{\alpha}_{n,j-M+\nu+1,l}\int_{0}^{\Delta t} K_{mn}\left(\frac{c}{\sigma}\left((M-\nu-1)\Delta t + \tau_k - s\right)\right)P_l(s)\,ds
\end{aligned}$$

$$= \sum_{\nu=\max(0,M-j)}^{M-2} \sum_{l=0}^{q-1} \widehat{\mathcal{L}}_{m,n,k,l,\nu} \widehat{\alpha}_{n,j-M+\nu+1,l}$$
$$= \sum_{\nu=\max(0,M-j)}^{M-2} \sum_{l=0}^{q-1} \mathcal{L}_{m,n,k,l,\nu} \alpha_{n,j-M+\nu+1,l}$$

where in the last two lines, we have again defined $\widehat{\mathcal{L}}$, and then $\mathcal{L}$, by precomposition with the discrete Legendre transform matrix. The Mp^2q^2 quantities $\mathcal{L}_{m,n,k,l,\nu}$ can be precomputed. As before, using (18), this only requires computing Mpq^2 integrals. Thus the cost of computing $L_{m,n,j,k}$ for each time step is $\mathcal{O}\left(Mp^2q^2\right)$.

3.3. The history term

A naive treatment of the history term would simply amount to extending the local integral back to $t = 0$ rather than $t = t_j^*$, and using the same method. This would require summing over the full history of the numerical solution $\alpha_{n,j,l}$ at each time step, rather than at most the previous $M - 1$ time steps, as well as precomputing Npq^2 rather than Mpq^2 integrals. We can avoid this expense with the sum-of-exponentials history compression technique, which has been used in a variety of contexts to compress and efficiently update the history contribution of Volterra integral operators [14,19,21,23]. The following discussion illustrates the technique.

We assume for now that there is a sum-of-exponentials representation of the kernel K_{mn},

$$K_{mn}(t) = \sum_{\mu=1}^{n_e} w_{m,n,\mu} e^{-\lambda_\mu t}, \tag{22}$$

valid for $\delta \le \sqrt{2}t \le t_{\max}$, with $0 < \delta < t_{\max}$. Here $w_{m,n,\mu}, \lambda_\mu \in \mathbb{C}$ and $\operatorname{Re}\lambda_\mu \ge 0$. We will show in Section 4.1 that such a representation can be constructed with $\delta = 20$, $t_{\max} = 10^8$, and $n_e = 67$, which is accurate to near machine precision for all m, n.

Let us assume $T \le \sigma t_{\max}/(\sqrt{2}c)$, and choose M such that $(M-1)\Delta t \ge \sigma\delta/(\sqrt{2}c)$. If $j \le M$, we have $t_j^* = 0$ and $H_{m,n,j,k} = 0$. Otherwise, we have $j \ge M + 1$, so that

$$\begin{aligned} H_{m,n,j,k} &= \int_0^{(j-M)\Delta t} K_{mn}\left(\frac{c}{\sigma}\left(t_{jk} - s\right)\right) \alpha_n(s)\, ds \\ &= \sum_{\mu=1}^{n_e} w_{m,n,\mu} \int_0^{(j-M)\Delta t} e^{-c\lambda_\mu (t_{jk}-s)/\sigma} \alpha_n(s)\, ds \\ &= \sum_{\mu=1}^{n_e} w_{m,n,\mu} h_{n,j,k,\mu} \end{aligned} \tag{23}$$

where $h_{n,j,k,\mu} = \int_0^{(j-M)\Delta t} e^{-c\lambda_\mu (t_{jk}-s)/\sigma} \alpha_n(s)\, ds$. Observe that

$$\begin{aligned} h_{n,j,k,\mu} &= \int_0^{(j-M)\Delta t} e^{-c\lambda_\mu (t_{jk}-s)/\sigma} \alpha_n(s)\, ds \\ &= e^{-c\lambda_\mu \Delta t/\sigma} \int_0^{(j-1-M)\Delta t} e^{-c\lambda_\mu (t_{(j-1)k}-s)/\sigma} \alpha_n(s)\, ds + \int_{(j-1-M)\Delta t}^{(j-M)\Delta t} e^{-c\lambda_\mu (t_{jk}-s)/\sigma} \alpha_n(s)\, ds \\ &= e^{-c\lambda_\mu \Delta t/\sigma} h_{n,j-1,k,\mu} + \int_{(j-1-M)\Delta t}^{(j-M)\Delta t} e^{-c\lambda_\mu (t_{jk}-s)/\sigma} \alpha_n(s)\, ds. \end{aligned}$$

This is a recurrence for $h_{n,j,k,\mu}$. To update it from one time step to the next, we multiply by a damping factor and add a local update integral. For the local update integral, we write

$$\int_{(j-1-M)\Delta t}^{(j-M)\Delta t} e^{-c\lambda_\mu (t_{jk}-s)/\sigma} \alpha_n(s)\, ds = \sum_{l=0}^{q-1} \widehat{\alpha}_{n,j-M,l} \int_{(j-1-M)\Delta t}^{(j-M)\Delta t} e^{-c\lambda_\mu (t_{jk}-s)/\sigma} P_l^{j-M}(s)\, ds$$

$$
\begin{aligned}
&= \sum_{l=0}^{q-1} \widehat{\alpha}_{n,j-M,l} \int_0^{\Delta t} e^{-c\lambda_\mu (M\Delta t + \tau_k - s)/\sigma} P_l(s)\, ds \\
&= \sum_{l=0}^{q-1} \widehat{\mathcal{H}}_{k,l,\mu} \widehat{\alpha}_{n,j-M,l} \\
&= \sum_{l=0}^{q-1} \mathcal{H}_{k,l,\mu} \alpha_{n,j-M,l},
\end{aligned}
$$

where the second to last line defines $\widehat{\mathcal{H}}_{k,l,\mu}$, and $\mathcal{H}_{k,l,\mu}$ is again obtained from $\widehat{\mathcal{H}}_{k,l,\mu}$ by precomposition with the discrete Legendre transform matrix. The $n_e q^2$ quantities $\mathcal{H}_{k,l,\mu}$ can be precomputed. We obtain

$$
h_{n,j,k,\mu} = e^{-c\lambda_\mu \Delta t/\sigma} h_{n,j-1,k,\mu} + \sum_{l=0}^{q-1} \mathcal{H}_{k,l,\mu} \alpha_{n,j-M,l} \tag{24}
$$

which, combined with (23), completes our treatment of the history term. The cost of updating $h_{n,j,k,\mu}$ at each time step using (24) is $\mathcal{O}\left(pq^2 n_e\right)$, and the cost of computing $H_{m,n,j,k}$ from these values is $\mathcal{O}\left(p^2 q n_e\right)$. For comparison, the cost of computing $H_{m,n,j,k}$ directly at each time step, using the same method as we use for the local term, would be $\mathcal{O}\left(p^2 q^2 N\right)$, in addition to the significantly larger precomputation cost.

3.4. Summary of the time-stepping procedure and computational complexity

We can now summarize the full solver. We first precompute and store the quantities $\mathcal{C}_{m,n,k,l}$, $\mathcal{L}_{m,n,k,l,\nu}$, and $\mathcal{H}_{k,l,\mu}$. Now let

$$
b_{m,j,k} = -\frac{g^2}{2\pi c} \sum_{n=1}^{p} \left(L_{m,n,j,k} + H_{m,n,j,k}\right) + f_m(t_{jk})
$$

be the right hand side of (20). Sections 3.2 and 3.3 describe how to compute $b_{m,j,k}$ at each time step using the precomputed arrays and the values of the solution at the previous M time steps. Using this and (21), we can write the discretized VIE (20) as

$$
\alpha_{m,j,k} + \frac{g^2}{2\pi c} \sum_{n=1}^{p} \sum_{l=0}^{q} \mathcal{C}_{m,n,k,l} \alpha_{n,j,l} = b_{m,j,k}.
$$

To take the jth time step, we solve this $pq \times pq$ linear system. The system matrix, with entries $\delta_{mn}\delta_{kl} + \mathcal{C}_{m,n,k,l}$, can be formed and LU-factorized as a precomputation.

The cost of computing $b_{m,j,k}$ at each time step is $\mathcal{O}\left(p^2 q^2 M + (p^2 q + pq^2) n_e\right)$, ignoring the evaluation of $f_m(t)$. The cost of solving the linear system by backward substitution is just $\mathcal{O}\left(p^2 q^2\right)$. Let us write the computational complexity in terms of the number of time steps, N. There are two $N \to \infty$ regimes: T fixed, $\Delta t \to 0$, and Δt fixed, $T \to \infty$. In practice, using high-order time-stepping, convergence with respect to Δt is rapid, and the limit $\Delta t \to 0$ is unimportant; see Figs. 6 and 10 in Section 5. With Δt fixed and $T \to \infty$, M is fixed, and the computational complexity is $\mathcal{O}(N n_e)$. n_e in turn depends on $t_{\max}$, and in particular, as we will discuss later, grows like $\mathcal{O}(\log t_{\max})$. To ensure $T = N\Delta t \leq t_{\max}/\sqrt{2}$, then, we have $n_e = \mathcal{O}(\log N)$, giving overall $\mathcal{O}(N \log N)$ computational complexity.

4. Representation and evaluation of kernels

We have seen that building the arrays $\mathcal{C}_{m,n,k,l}$ and $\mathcal{L}_{m,n,k,l,\nu}$ requires computing integrals against the kernels k_n. In particular, if we use standard integration routines, we require a method of evaluating those kernels for all $t \geq 0$. Furthermore, evolving the history term requires a sum-of-exponentials representation (22) of K_{mn}, valid for sufficiently large times.

We will accomplish both objectives by using an efficient representation of the kernel j_n, defined by (16). First, we will obtain a sum-of-exponentials representation of j_n, valid when $t > \delta = 20$, and use it to obtain similar representations for k_n and hence K_{mn}. This also solves the problem of evaluating k_n for sufficiently large t. Then we will obtain Chebyshev expansions of j_n and thereby of k_n valid for $t \leq \delta$.

Fig. 1 shows representative examples of the kernels $j_n(t)$ for $t \in [0, 20]$ and $t > 20$.

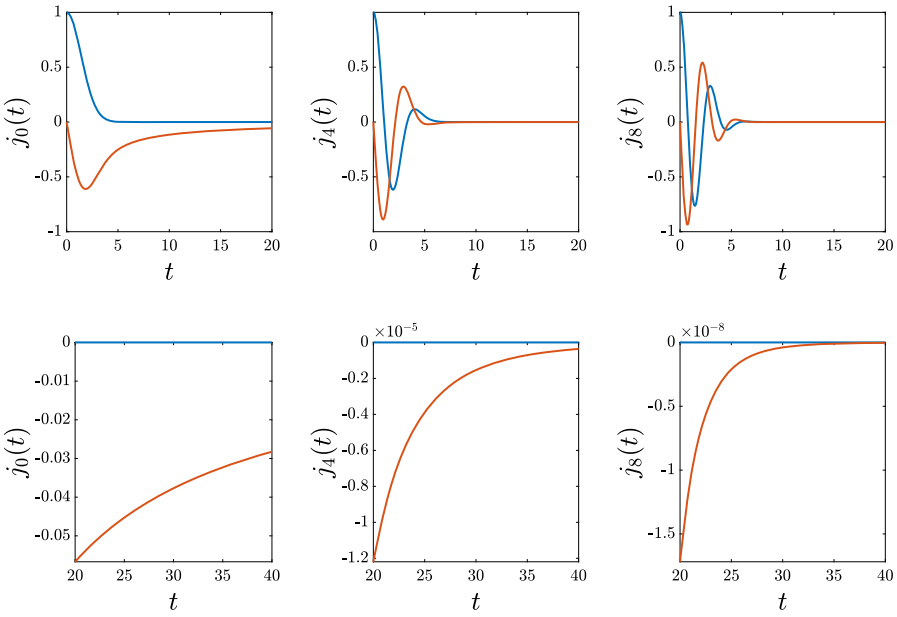

Fig. 1. The first row shows $j_n(t)$ for $n = 0, 4, 8$, and t in the small-time interval $[0, 20]$. Re $j_n(t)$ is indicated by the blue curve, and Im $j_n(t)$ by the red curve. In this interval, we represent each j_n by a Chebyshev expansion. The second row shows the same kernels for $t > 20$, where we represent them by sum-of-exponentials expansions. (For interpretation of the colors in the figure(s), the reader is referred to the web version of this article.)

4.1. Sum-of-exponentials representation for large times

We start by constructing a sum-of-exponentials representation of $j_n(t)$ valid for $t > \delta$, for some $\delta > 0$ to be determined. We note that a sum-of-exponentials representation (22) of K_{mn} can then be obtained from (17) and (18). In particular, suppose the representation

$$j_n(t) = \sum_{\mu=1}^{n_e} \widetilde{w}_{n,\mu} e^{-\widetilde{\lambda}_\mu t} \tag{25}$$

is valid for $t > \delta$, for $\widetilde{w}_{n,\mu} \in \mathbb{C}$ and $\widetilde{\lambda}_\mu > 0$. Then for $t \geq \delta/\sqrt{2}$, when $m+n$ is even, we have

$$\begin{aligned}
K_{mn}(t) &= K_{mn}\left(\delta/\sqrt{2}\right) + (-1)^m (-i)^{m+n} \frac{\Gamma\left(\frac{m+n+1}{2}\right)}{\sqrt{\frac{m!n!}{2}}} \int_{\delta/\sqrt{2}}^{t} e^{i\frac{\Omega\sigma}{c}s} j_{m+n}(\sqrt{2}s)\, ds \\
&= K_{mn}\left(\delta/\sqrt{2}\right) + (-1)^m (-i)^{m+n} \frac{\Gamma\left(\frac{m+n+1}{2}\right)}{\sqrt{\frac{m!n!}{2}}} \sum_{\mu=1}^{n_e} \widetilde{w}_{n,\mu} \int_{\delta/\sqrt{2}}^{t} e^{\left(i\frac{\Omega\sigma}{c} - \sqrt{2}\widetilde{\lambda}_\mu\right)s} ds \\
&= K_{mn}\left(\delta/\sqrt{2}\right) + (-1)^m (-i)^{m+n} \frac{\Gamma\left(\frac{m+n+1}{2}\right)}{\sqrt{\frac{m!n!}{2}}} \sum_{\mu=1}^{n_e} \frac{\widetilde{w}_{n,\mu}}{i\Omega\sigma/c - \sqrt{2}\widetilde{\lambda}_\mu} \\
&\quad \times \left(e^{\left(i\frac{\Omega\sigma}{c} - \sqrt{2}\widetilde{\lambda}_\mu\right)t} - e^{\left(i\frac{\Omega\sigma}{c} - \sqrt{2}\widetilde{\lambda}_\mu\right)\delta/\sqrt{2}} \right) \\
&= \sum_{\mu=1}^{n_e+1} w_{m,n,\mu} e^{-\lambda_\mu t}
\end{aligned}$$

with

$$w_{m,n,\mu} = \begin{cases} (-1)^m (-i)^{m+n} \frac{\Gamma\left(\frac{m+n+1}{2}\right)}{\sqrt{\frac{m!n!}{2}}} \frac{\widetilde{w}_{n,\mu}}{i\Omega\sigma/c - \sqrt{2}\widetilde{\lambda}_\mu} & \text{if } 1 \leq \mu \leq n_e \\ K_{mn}\left(\delta/\sqrt{2}\right) - (-1)^m (-i)^{m+n} \frac{\Gamma\left(\frac{m+n+1}{2}\right)}{\sqrt{\frac{m!n!}{2}}} \sum_{\nu=1}^{n_e} \frac{\widetilde{w}_{n,\nu}}{i\Omega\sigma/c - \sqrt{2}\widetilde{\lambda}_\nu} e^{\left(i\frac{\Omega\sigma}{c} - \sqrt{2}\widetilde{\lambda}_\nu\right)\delta/\sqrt{2}} & \text{if } \mu = n_e + 1 \end{cases}$$

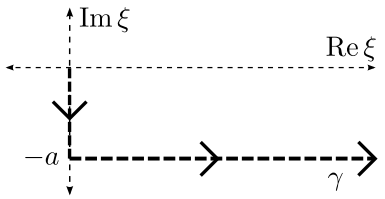

Fig. 2. Contour of integration used for $J_{mn}(t)$ to obtain sum-of-exponentials representation. For sufficiently large a and δ, the contribution from the horizontal part of the contour is negligible when $t > \delta$. The sum-of-exponentials representation is obtained by applying a quadrature rule to the vertical part.

and

$$\lambda_\mu = \begin{cases} \sqrt{2\widetilde{\lambda}_\mu} - i\Omega\sigma/c & \text{if } 1 \le \mu \le n_e \\ 0 & \text{if } \mu = n_e + 1. \end{cases}$$

Redefining $n_e \leftarrow n_e + 1$ gives the desired representation (22). We focus then on the construction of (25).

We begin by deforming the integral defining j_n in (16) from the interval $[0, \infty)$ to the contour γ shown in Fig. 2. That is, we have

$$\begin{aligned} j_n(t) &= \frac{2}{\Gamma\left(\frac{n+1}{2}\right)} \left((-i)^{n+1} \int_0^a \eta^n e^{\eta^2 - \eta t}\, d\eta + \int_0^\infty (\eta - ia)^n e^{-(\eta - ia)^2 - i(\eta - ia)t}\, d\eta \right) \\ &\equiv j_n^{(1)}(t) + j_n^{(2)}(t). \end{aligned}$$

We show in Appendix A that

$$\left| j_n^{(2)}(t) \right| \le 14 e^{2a^2 - at}.$$

If we take $a = \delta/4$, then $\left| j_n^{(2)}(t) \right| \le 14 e^{-\delta^2/8}$ when $t \ge \delta$. Thus, to ensure $\left| j_n^{(2)}(t) \right| < \varepsilon$ for all $t \ge \delta$, we can take $\delta > \sqrt{8 \log(14/\varepsilon)}$. If ε is the double machine precision, then taking $\delta = 20$, $a = 5$ is sufficient to neglect $\left| j_n^{(2)}(t) \right|$.

As a consequence, if we can find a quadrature rule $\{\omega_{n,\mu}, \widetilde{\lambda}_\mu\}_{\mu=1}^{n_e}$ so that

$$j_n^{(1)}(t) = \frac{2(-i)^{n+1}}{\Gamma\left(\frac{n+1}{2}\right)} \int_0^a \eta^n e^{\eta^2 - \eta t}\, d\eta \approx \sum_{\mu=1}^{n_e} \omega_{n,\mu} \widetilde{\lambda}_\mu^n e^{\widetilde{\lambda}_\mu^2 - \widetilde{\lambda}_\mu t}$$

holds to high accuracy for all $t \ge \delta$, then this gives (25) with

$$\widetilde{w}_{n,\mu} = \omega_{n,\mu} \widetilde{\lambda}_\mu^n e^{\widetilde{\lambda}_\mu^2}.$$

When $n > 23$, $|j_n(t)|$ is below the double machine precision for all $t > 20$. We therefore only need quadratures for the above integrals which are valid for $n = 0, \ldots, 23$; we can simply take $\omega_{n,\mu} = 0$ for $n \ge 24$.

The method of generalized Gaussian quadrature can be used to find such a quadrature rule [27]. Given a family of functions – in this case, the functions $\eta^n e^{\eta^2 - \eta t}$, $\eta \in [0, 5]$, for $n = 0, \ldots, 23$ and $\delta < t < t_{\max}$ – this method uses a nonlinear optimization process to determine a minimal set of quadrature nodes and weights sufficient to integrate all functions in the family to near machine precision. An upper bound on the number of quadrature nodes required can be given in terms of the numerical rank of the family of functions. It is straightforward to adapt the proof given in Ref. [28, Lemma 4.4] for the case of a family of decaying exponentials to the present setting. Briefly, the proof works by 1) rescaling the interval to $[0, 1]$; 2) discretizing $[0, 1]$ by a composite Chebyshev grid with nodes exponentially clustered at the origin; and 3) using standard error estimates for Chebyshev interpolation to show that the resulting piecewise polynomial approximation is uniformly accurate for all functions in the family. This argument shows that the numerical rank of the family scales as $\mathcal{O}(\log(t_{\max}/\delta))$. In practice, we simply take $t_{\max} = 10\,000\,000$, several orders of magnitude larger than is needed for the examples shown in this article, and obtain a quadrature rule of $n_e = 67$ nodes and weights.

4.2. Chebyshev representation for small times

We next consider the evaluation of $k_n(t)$ for $t \le \delta/\sqrt{2}$. First, we can evaluate each $j_n(t)$ at Chebyshev nodes on $[0, \delta]$ using adaptive integration. $j_n(t)$ is an entire function, so its Chebyshev interpolant converges super-exponentially [29]. A moderate number of Chebyshev nodes are therefore sufficient to represent the function on the full interval to near machine

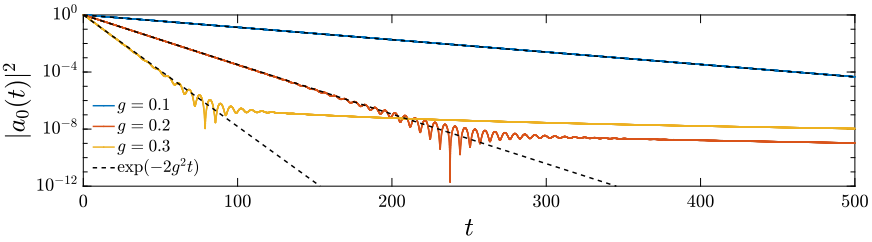

Fig. 3. $|a_0(t)|^2$ for the first example with $p = 1$ and several choices of g, along with the expected initial decay curve.

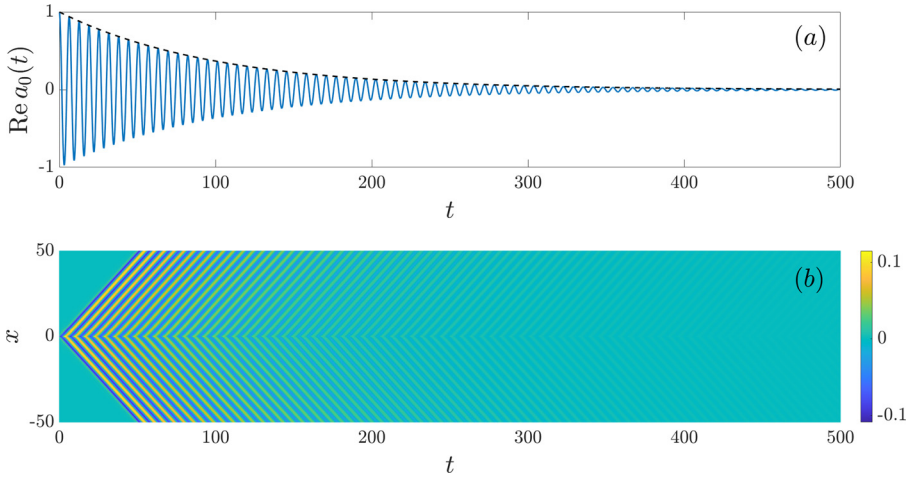

Fig. 4. (a) $\mathrm{Re}\, a_0(t)$ and (b) $\mathrm{Re}\, u(x,t)$ for the first example with $p = 1$ and $g = 0.1$. In (a), the black dashed line is the curve $\exp(-g^2t)$.

precision by its interpolant at these nodes; see Fig. 1 for plots of some $j_n(t)$ on $[0, \delta]$. The samples at Chebyshev nodes can be computed once and stored. $j_n(t)$ can then be evaluated at any $t \in [0, \delta]$ by barycentric interpolation [29–31].

Given Ω, c, and σ, samples of the integrand of $k_n(t)$ in (17) at Chebyshev nodes on $[0, \delta/\sqrt{2}]$ can then be obtained by pointwise multiplication. If $\Omega\sigma/c$ is large, then to resolve the complex exponential, j_n can be evaluated on a denser Chebyshev grid. Accurate samples of $k_n(t)$ at the same Chebyshev nodes can then be obtained by spectral integration [32], and as before, can be used to represent $k_n(t)$ on $[0, \delta/\sqrt{2}]$ by barycentric interpolation.

5. Numerical results

We demonstrate the solver using two examples. In the first, we place an atom in its excited state and observe its decay. In the second, we excite the atom with a wavepacket.

5.1. Example 1: decay of an excited atom

The first example is characterized by the initial condition

$$a(x, 0) = 1, \quad u(x, 0) = 0,$$

which corresponds to taking $\alpha_m(0) = \delta_{0n}$ and $U_m(t) = 0$ in (10). We take $c = \Omega = 1$ and $\sigma = 0.1$.

We first represent the solution using only a single Hermite polynomial, $p = 1$. Fig. 3 shows $|a_0(t)|^2$ for $g = 0.1, 0.2, 0.3$. The solutions are characterized by an initial exponential decay regime, with the decay rate determined by g, followed by a tail of significantly slower decay. The plots indicate close agreement with the standard Wigner-Weisskopf estimate $|a_0(t)|^2 \approx e^{-2g^2t}$ of the initial decay rate; for a derivation in the three-dimensional case, which is straightforwardly adapted to the one-dimensional case, we refer to [9].

Fig. 4 shows $\mathrm{Re}\, a_0(t)$ and $\mathrm{Re}\, u(x,t)$ for $g = 0.1$. As the atom amplitude decays, it acts as a source for the photon field, which resembles a wave of speed c radiating from the origin. We note that the photon amplitude is not identically zero outside of the light cone associated with speed c. Rather, as a result of nonlocal effects arising from the fractional Laplacian term of (1), it decays algebraically outside of the light cone.

We next consider the limit of a large number of Hermite polynomials, $p \to \infty$. To do so, we increase p until the first five non-zero coefficients a_n are converged to high accuracy (we note that, as a result of the symmetry of the system about the

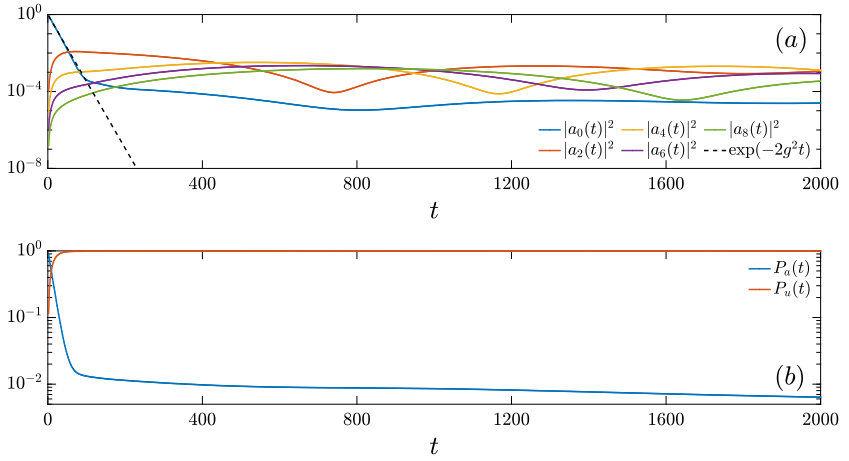

Fig. 5. (a) $|a_n(t)|^2$ with $n = 0, 2, \ldots, 8$ for the first example with $p = 40$ and $g = 0.2$. (b) The total probability associated with the atom and the photon field.

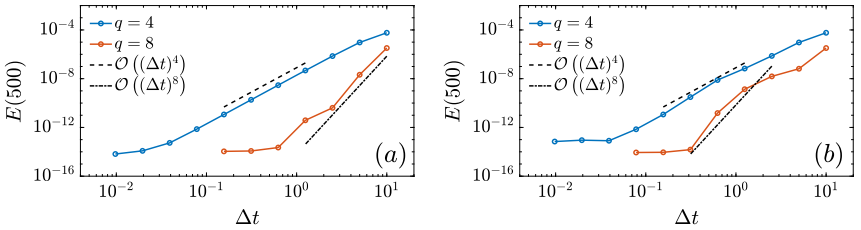

Fig. 6. Error $E(t)$ for the first example with $g = 0.2$ for (a) $p = 1$ and (b) $p = 40$, using fourth and eighth-order time-stepping.

origin, the odd coefficients are identically zero). $p = 40$ was sufficient for the simulations considered here. We fix $g = 0.2$, so our results can be compared with the red curve in Fig. 3. Fig. 5a shows $|a_n(t)|^2$ for the first five even Hermite polynomials. At very short times, the $n = 0$ coefficient decays with the same rate as in the $p = 1$ case. However, the rapid decay regime ends sooner, and gives way to complicated, long-lived dynamics among the coefficients of the various Hermite polynomials.

Another perspective is given by Fig. 5b, which shows the total probability associated with the atom and photon amplitudes. It can also be compared directly with the red curve in Fig. 3, since in the $p = 1$ case $|a_0(t)|^2 = P_a(t)$. Compared with the $p = 1$ case, in the $p = 40$ case the atom dissipates much less of its probability mass into the photon field.

Evidently, allowing multiple Hermite coefficients gives rise to a trapping effect, whereby some portion of the probability associated with the zero coefficient remains trapped in higher-order modes rather than being radiated into the continuum through the photon field. As the solution evolves in time, higher and higher-order coefficients become activated, and the total probability associated with the atomic amplitude decays exceptionally slowly, if at all.

The plot of the photon amplitude for the $p = 40$ case is qualitatively similar to that appearing in Fig. 4 for the $p = 1$ case, so we do not plot it. The main difference is that in the $p = 40$ case, the atom remains a longer-lived source of larger magnitude for the photon field.

We next verify the order of accuracy of the time-stepping algorithm by measuring the error

$$E(t) = \sqrt{\frac{1}{\sigma}\int_{-\infty}^{\infty} \left|a(x,t) - a^{\text{ref}}(x,t)\right| \rho(x/\sigma)\, dx} = \sqrt{\sum_{n=0}^{p-1} \left|\alpha_n(t) - \alpha_n^{\text{ref}}(t)\right|^2} \tag{26}$$

against a well-converged reference solution a^{ref} with Hermite coefficients α_n^{ref}. We take the parameters as above with $g = 0.2$, and measure the error $E(t)$ at $t = 500$ using the fourth and eighth-order methods; $q = 4$ and $q = 8$, respectively. Fig. 6a gives results for the $p = 1$ case, and Fig. 6b for $p = 40$.

5.2. Example 2: response to a photon pulse

Our second example models the response of the atom to a photon pulse. We take

$$u_0(x) = \left(\frac{2}{\pi\beta^2}\right)^{1/4} e^{-(x-x_0)^2/\beta^2} e^{i\xi_0 x} \tag{27}$$

with x_0, β, and ξ_0 the inital wavepacket center, width, and wavenumber, respectively. The normalization ensures $\int_{-\infty}^{\infty} |u_0(x)|^2\, dx = 1$. The free evolution is given by

$$\begin{aligned} U(x,t) &= \int_{-\infty}^{\infty} G(x-y,t)u_0(y)\,dy \\ &= \frac{1}{2\pi}\int_{-\infty}^{\infty} \widehat{G}(\xi,t)e^{i\xi x}\widehat{u_0}(\xi)\,d\xi \\ &= \frac{\sqrt{\beta}}{(2\pi)^{3/4}}\int_{-\infty}^{\infty} e^{-i(c|\xi|t-\xi x+x_0(\xi-\xi_0))}e^{-(\xi-\xi_0)^2\beta^2/4}\,d\xi. \end{aligned}$$

If we take ξ_0, β sufficiently large so that $\varepsilon > \frac{\sqrt{\beta}}{(2\pi)^{3/4}}\int_{-\infty}^{0} e^{-(\xi-\xi_0)^2\beta^2/4} = \frac{\operatorname{erfc}(\beta\xi_0/2)}{(8\pi\beta^2)^{1/4}}$ for some ε, then up to an error ε, we simply recover a translation of the initial wavepacket:

$$U(x,t) \approx \frac{\sqrt{\beta}}{(2\pi)^{3/4}}e^{ix_0\xi_0}\int_{-\infty}^{\infty} e^{i\xi(x-x_0-ct)}e^{-(\xi-\xi_0)^2\beta^2/4}\,d\xi = u_0(x-ct).$$

Thus the free evolution of a wavepacket with a sufficiently high frequency modulation relative to its width is approximately given by translation at velocity c. We will choose ξ_0, β so that the approximate equality holds to machine precision – $\xi_0\beta \geq 12$ with $\beta \geq 1$ is sufficient – and for simplicity take it to be an equality going forward.

To compute the source term in the VIE (10), we write

$$\int_0^t e^{i\Omega s}\widehat{u_m}(s)\,ds = \frac{1}{\sigma}\int_{-\infty}^{\infty} \rho(x/\sigma)f_m(x/\sigma)\int_0^t e^{i\Omega s}U(x,s)\,ds\,dx. \tag{28}$$

We have

$$\begin{aligned} \int_0^t e^{i\Omega s}U(x,s)\,ds &= \int_0^t e^{i\Omega s}u_0(x-cs)\,ds \\ &= \left(\frac{2}{\pi\beta^2}\right)^{1/4} e^{i\xi_0 x}\int_0^t e^{i(\Omega-\xi_0 c)s}e^{-(x-x_0-cs)^2/\beta^2}\,ds \\ &= \frac{i\pi^{1/4}\sqrt{\beta}}{2^{3/4}c}e^{i(\xi_0 x_0+\Omega(x-x_0)/c)}e^{-\frac{\beta^2(\Omega-\xi_0 c)^2}{4c^2}}\left(\operatorname{erfi}\left(\frac{\beta(\Omega-\xi_0 c)}{2c}-i\frac{x-x_0}{\beta}\right)\right. \\ &\quad \left.-\operatorname{erfi}\left(\frac{\beta(\Omega-\xi_0 c)}{2c}-i\frac{x-x_0-ct}{\beta}\right)\right). \end{aligned}$$

The outer integral in (28) can be computed at each time step by adaptive integration using the explicit expression for the inner integral. To improve the efficiency, the integrals for each m can be computed simultaneously using the recurrence for the normalized Hermite functions:

$$\sqrt{\frac{m+1}{2}}f_{m+1}(x) = xf_m(x) - \sqrt{\frac{m}{2}}f_{m-1}(x).$$

In this setup, we take $a(x,0) = 0$, with $c = \Omega = 1$ and $\sigma = 0.1$ as before, and we fix $g = 0.2$. We take $\beta = 12$ and $\mu = -80$ in (27), so that, to machine precision, the wavepacket does not initially overlap with the atomic density.

We first consider the single coefficient case $p = 1$. In Fig. 7, we plot $|a(t)|^2$ for different choices of the wavenumber, $\xi_0 = 0.4, 0.7, 1, 1.3, 1.6$. The incoming wavepacket interacts with the atom, increasing the magnitude of the atom amplitude, which then decays at the expected rate. We note that in this case, the rapid decay regime continues for longer than in the first example; a comparison can be made with the red curve in Fig. 3. We also see that a wavepacket with $\xi_0 = \Omega$ – exactly resonant with the atom – yields the largest and most long-lived atomic excitation. By contrast, when the modulation is chosen off-resonance, the atomic amplitude first follows the profile of the wavepacket-induced forcing before eventually settling into the usual decay regime.

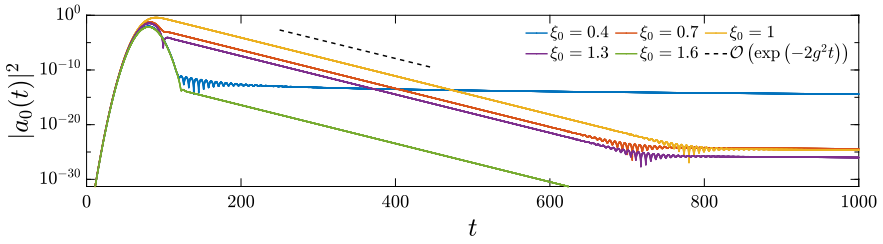

Fig. 7. $|a_0(t)|^2$ for the second example with $p = 1$ and several choices of ξ_0, along with an indication of the decay rate expected for an initially excited atom. The atomic resonance frequency is $\Omega = 1$.

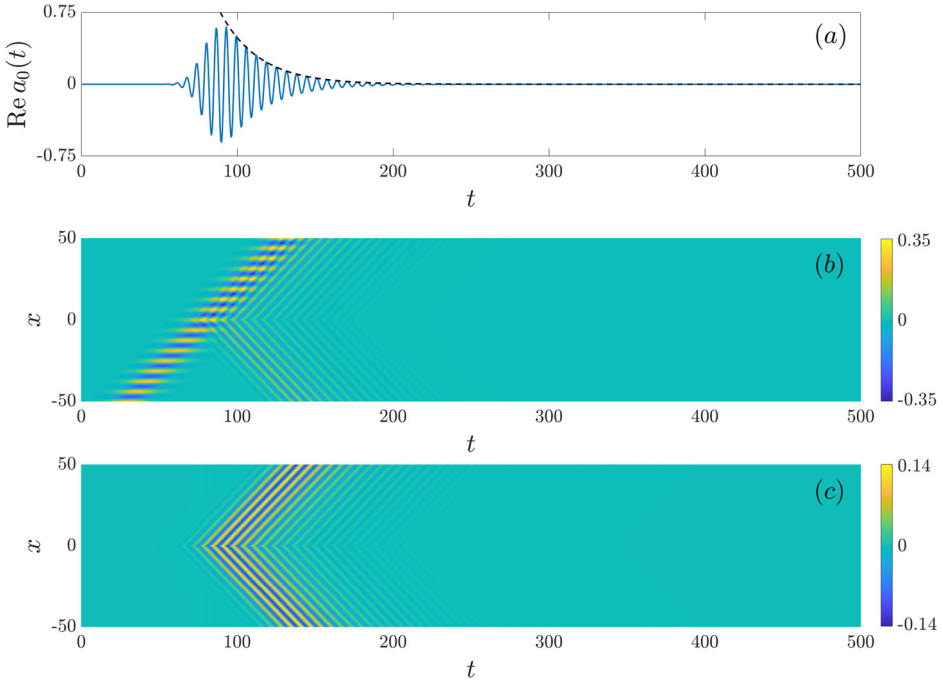

Fig. 8. (a) $\mathrm{Re}\, a_0(t)$, (b) $\mathrm{Re}\, u(x,t)$, and (c) $\mathrm{Re}\,(u(x,t) - U(x,t))$ for the second example with $p = 1$ and $\xi_0 = 1$. In (a), the black dashed line is the curve $\exp\left(-g^2(t - t_0)\right)$ with t_0 chosen to follow the envelope of the oscillation.

For the on-resonance case, $\xi_0 = 1$, Figs. 8a and 8b give plots of $\mathrm{Re}\, a(t)$ and $\mathrm{Re}\, u(x,t)$, respectively. We see the wavepacket approach the atom center and excite the atom, which then decays and induces its own response in the photon amplitude, given by $u - U$. Fig. 8c gives a plot of $\mathrm{Re}\,(u(x,t) - U(x,t))$.

We lastly consider the $p = 40$ case—this is again sufficient to achieve convergence to high accuracy for the first five non-zero a_n—for $\xi_0 = 1$. The results are given in Fig. 9, and are similar to those shown in Fig. 5. After the initial excitation, the behavior of the various Hermite modes comprising the atom amplitude is nearly identical to that shown in Fig. 5a for the first example. The behavior of the atomic and photonic contributions to the total probability are similar, except in this case the photonic probability contains contributions both from the incoming wavepacket and from the field induced by the decaying atom.

We again verify the order of accuracy of the fourth and eighth-order time-stepping algorithms by measuring the error $E(t)$, defined by (26), for $t = 250$, with $g = 0.2$ and $\xi_0 = 1$. Results for the $p = 1$ case are given in Fig. 10a, and for the $p = 40$ case in Fig. 10b.

6. Conclusion

We have presented an efficient numerical method to solve (1) by reformulating it as an integro-differential equation. This avoids the challenges associated with the nonlocality of the differential operator, and the unboundedness of the domain. We address the resulting Volterra-type memory dependence, for the case of a Gaussian atomic density, by projecting the solution history onto a collection of exponentials, which can be propagated by a simple recurrence.

In our numerical experiments, when the spatial extent of the atom amplitude is represented by a single degree of freedom, we recover the expected Wigner-Weisskopf decay behavior for a one-atom system. When multiple degrees of freedom

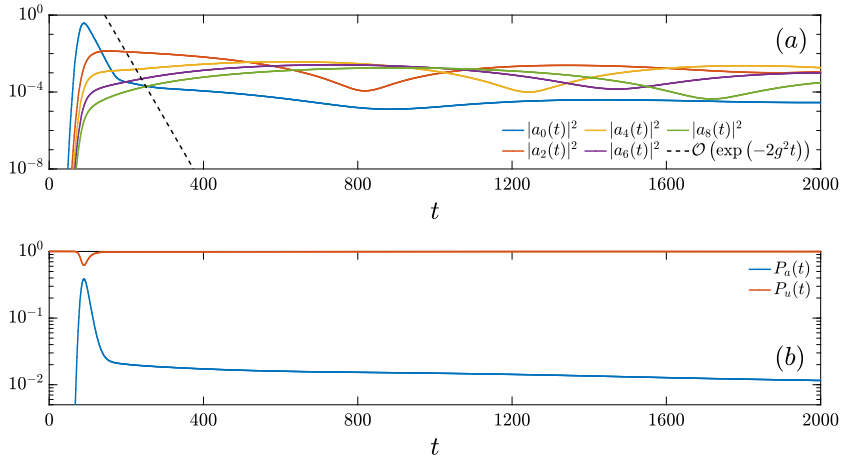

Fig. 9. (a) $|a_n(t)|^2$ with $n = 0, 2, \ldots, 8$ for the second example with $p = 40$ and $\xi_0 = 1$, along with an indication of the decay rate expected for an initially excited atom. (b) The total probability associated with the atom and the photon field.

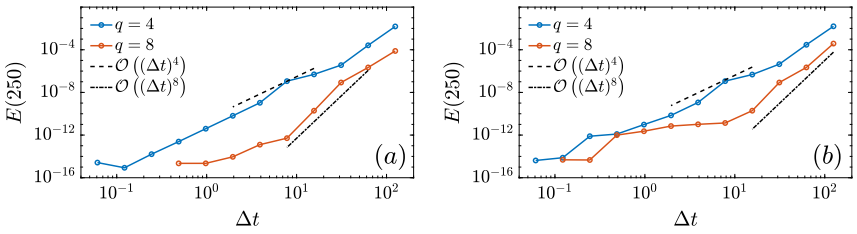

Fig. 10. Error $E(t)$ for the second example with $\xi_0 = 1$ for (a) $p = 1$ and (b) $p = 40$, using fourth and eighth-order time-stepping.

are included, we observe more complicated collective dynamics. Our numerical method serves as a useful starting point to examine more complicated systems and related models in quantum optics. In particular, in a forthcoming publication, we will generalize the method to systems of distinct two-level atoms coupled to a photon field.

CRediT authorship contribution statement

All authors contributed equally to all parts of this work.

Declaration of competing interest

The authors declare that they have no known competing financial interests or personal relationships that could have appeared to influence the work reported in this paper.

Data availability

Data will be made available on request.

Acknowledgements

John Schotland was supported in part by the NSF grant DMS-1912821 and the AFOSR grant FA9550-19-1-0320. The Flatiron Institute is a division of the Simons Foundation.

Appendix A. Estimate of $j_n^{(2)}(t)$

In this Appendix, we prove the estimate used to neglect $j_n^{(2)}(t)$ in Section 4.1. We have

$$\frac{\Gamma\left(\frac{n+1}{2}\right)}{2}\left|j_n^{(2)}(t)\right| = \left|\int_0^\infty (\eta - ia)^n e^{-(\eta-ia)^2 - i(\eta-ia)t}\, d\eta\right|$$

$$\leq e^{a^2-at}\int_0^\infty \left(\eta^2+a^2\right)^{n/2} e^{-\eta^2}\,d\eta$$

$$= e^{2a^2-at}\int_a^\infty \frac{x^{n+1}}{\sqrt{x^2-a^2}} e^{-x^2}\,dx,$$

where in the last line we have made the change of variables $x^2=\eta^2+a^2$. We split the integral into two pieces:

$$\int_a^\infty \frac{x^{n+1}}{\sqrt{x^2-a^2}} e^{-x^2}\,dx = \left(\int_a^{\sqrt{2}a} + \int_{\sqrt{2}a}^\infty\right) \frac{x^{n+1}}{\sqrt{x^2-a^2}} e^{-x^2}\,dx = I_1 + I_2.$$

For the first integral, we have

$$I_1 \leq 2^{(n+1)/2} a^{n+1} e^{-a^2} \int_a^{\sqrt{2}a} \left(x^2-a^2\right)^{-1/2}\,dx.$$

The integral can be computed by the substitution $x = a\sec\theta$, and is equal to $\log\left(1+\sqrt{2}\right)$. We also use the estimate $a^{n+1}e^{-a^2} \leq \sqrt{\frac{n+1}{2}}$ to obtain

$$I_1 \leq 2^{n/2}\sqrt{n+1}\log\left(1+\sqrt{2}\right).$$

For the second integral, we use that $\frac{x}{\sqrt{x^2-a^2}} \leq \sqrt{2}$ when $x \geq \sqrt{2}a$ to obtain

$$I_2 \leq \sqrt{2}\int_{\sqrt{2}a}^\infty x^n e^{-x^2}\,dx \leq \sqrt{2}\int_0^\infty x^n e^{-x^2}\,dx = \frac{\Gamma\left(\frac{n+1}{2}\right)}{\sqrt{2}}.$$

Combining these results gives the desired result,

$$\left|j_n^{(2)}(t)\right| \leq e^{2a^2-at}\left(\log\left(1+\sqrt{2}\right)\frac{2^{\frac{n}{2}+1}\sqrt{n+1}}{\Gamma\left(\frac{n+1}{2}\right)} + \sqrt{2}\right) \leq 14 e^{2a^2-at}.$$

In the last inequality, we have used that $\frac{2^{\frac{n}{2}}\sqrt{n+1}}{\Gamma\left(\frac{n+1}{2}\right)}$ reaches its maximum of approximately 6.9 at $n=5$.

References

[1] S. Haroche, J. Raimond, Exploring the Quantum: Atoms, Cavities and Photons, Oxford University Press, 2006.
[2] C. Gardiner, P. Zoller, The Quantum World of Ultra-Cold Atoms and Light Book I: Foundations of Quantum Optics, Imperial College Press, 2014.
[3] Z. Liao, X. Zeng, H. Nha, M.S. Zubairy, Photon transport in a one-dimensional nanophotonic waveguide QED system, Phys. Scr. 91 (6) (2016) 063004.
[4] D. Roy, C. Wilson, O. Firstenberg, Strongly interacting photons in one-dimensional continuum: colloquioum, Rev. Mod. Phys. 89 (2017) 021001.
[5] M. Kira, S.W. Koch, Semiconductor Quantum Optics, Cambridge University Press, 2009.
[6] H. Kimble, The quantum Internet, Nature 453 (7198) (2008) 1023–1030.
[7] H.D. Riedmatten, M. Afzelius, M. Staudt, C. Simon, N. Gisin, A solid-state light-matter interface at the single-photon level, Nature 456 (2008) 773–777.
[8] I. Bloch, J. Dalibard, S. Nascimbène, Quantum simulations with ultracold quantum gases, Nat. Phys. 8 (4) (2012) 267–276.
[9] J. Kraisler, J.C. Schotland, Collective spontaneous emission and kinetic equations for one-photon light in random media, J. Math. Phys. 63 (3) (2022) 031901.
[10] J.P. Boyd, Chebyshev and Fourier Spectral Methods, Courier Corporation, 2001.
[11] S. Blanes, P. Moan, Splitting methods for the time-dependent Schrödinger equation, Phys. Lett. A 265 (1–2) (2000) 35–42.
[12] E. Hairer, C. Lubich, M. Schlichte, Fast numerical solution of nonlinear Volterra convolution equations, SIAM J. Sci. Comput. 6 (3) (1985) 532–541.
[13] S. Veerapaneni, G. Biros, A high-order solver for the heat equation in 1D domains with moving boundaries, SIAM J. Sci. Comput. 29 (6) (2007) 2581–2606.
[14] S. Jiang, L. Greengard, S. Wang, Efficient sum-of-exponentials approximations for the heat kernel and their applications, Adv. Comput. Math. 41 (2015) 529–551.
[15] J. Wang, L. Greengard, S. Jiang, S. Veerapaneni, Fast integral equation methods for linear and semilinear heat equations in moving domains, arXiv: 1910.00755, 2019.
[16] J. Kaye, D. Golež, Low rank compression in the numerical solution of the nonequilibrium Dyson equation, SciPost Phys. 10 (2021) 91.
[17] J. Kaye, A. Barnett, L. Greengard, A high-order integral equation-based solver for the time-dependent Schrödinger equation, Commun. Pure Appl. Math. 75 (8) (2022) 1657–1712.
[18] J. Dölz, H. Egger, V. Shashkov, A fast and oblivious matrix compression algorithm for Volterra integral operators, Adv. Comput. Math. 47 (6) (2021) 1–24.

[19] B. Alpert, L. Greengard, T. Hagstrom, Rapid evaluation of nonreflecting boundary kernels for time-domain wave propagation, SIAM J. Numer. Anal. 37 (4) (2000) 1138–1164.
[20] C. Lubich, A. Schädle, Fast convolution for non–reflecting boundary conditions, SIAM J. Sci. Comput. 24 (1) (2002) 161–182.
[21] S. Jiang, L. Greengard, Fast evaluation of nonreflecting boundary conditions for the Schrödinger equation in one dimension, Comput. Math. Appl. 47 (6) (2004) 955–966.
[22] A. Schädle, M. López-Fernández, C. Lubich, Fast and oblivious convolution quadrature, SIAM J. Sci. Comput. 28 (2) (2006) 421–438.
[23] S. Jiang, L. Greengard, Efficient representation of nonreflecting boundary conditions for the time-dependent Schrödinger equation in two dimensions, Commun. Pure Appl. Math. 61 (2) (2008) 261–288.
[24] J. Kaye, L. Greengard, Transparent boundary conditions for the time-dependent Schrödinger equation with a vector potential, arXiv:1812.04200, 2018.
[25] I.S. Gradshteyn, I.M. Ryzhik, Table of Integrals, Series, and Products, 7th ed., Academic Press, 2007.
[26] W. Gautschi, The condition of Vandermonde-like matrices involving orthogonal polynomials, Linear Algebra Appl. 52–53 (1983) 293–300.
[27] J. Ma, V. Rokhlin, S. Wandzura, Generalized Gaussian quadrature rules for systems of arbitrary functions, SIAM J. Numer. Anal. 33 (3) (1996) 971–996.
[28] Z. Gimbutas, N.F. Marshall, V. Rokhlin, A fast simple algorithm for computing the potential of charges on a line, Appl. Comput. Harmon. Anal. 49 (3) (2020) 815–830.
[29] L.N. Trefethen, Approximation Theory and Approximation Practice, vol. 164, SIAM, 2019.
[30] J.-P. Berrut, L.N. Trefethen, Barycentric Lagrange interpolation, SIAM Rev. 46 (3) (2004) 501–517.
[31] N.J. Higham, The numerical stability of barycentric Lagrange interpolation, IMA J. Numer. Anal. 24 (4) (2004) 547–556.
[32] L. Greengard, Spectral integration and two-point boundary value problems, SIAM J. Numer. Anal. 28 (4) (1991) 1071–1080.